Since January 2020 Elsevier has created a COVID-19 resource centre with free information in English and Mandarin on the novel coronavirus COVID-19. The COVID-19 resource centre is hosted on Elsevier Connect, the company's public news and information website.

doi:10.1016/j.jmb.2009.05.080 J. Mol. Biol. (2009) 391, 518–535

JMB

Available online at www.sciencedirect.com

ScienceDirect

ELSEVIER

Solution Characterization of the Extracellular Region of CD147 and Its Interaction with Its Enzyme Ligand Cyclophilin A

Jennifer Schlegel[1], Jasmina S. Redzic[1], Christopher C. Porter[2], Vyacheslav Yurchenko[3], Michael Bukrinsky[4], Wladimir Labeikovsky[5], Geoffrey S. Armstrong[6], Fengli Zhang[7], Nancy G. Isern[8], James DeGregori[1], Robert Hodges[1] and Elan Zohar Eisenmesser[1]*

[1]*Department of Biochemistry and Molecular Genetics, University of Colorado Denver, School of Medicine, Aurora, CO 80045, USA*

[2]*Department of Pediatrics, University of Colorado Denver, School of Medicine, Aurora, CO 80045, USA*

[3]*Department of Pathology, Albert Einstein College of Medicine of Yeshiva University, 1300 Morris Park Ave, Bronx, NY 10461, USA*

[4]*Department of Immunology and Tropical Medicine, George Washington University, Washington, DC 20037, USA*

[5]*Laboratory of Cardiac/ Membrane Phisiology, The Rockefeller University, 1230 York Ave (box 297), New York, NY 10065, USA*

[6]*Department of Chemistry and Biochemistry, University of Colorado at Boulder, Boulder, CO 80309, USA*

[7]*National High Magnetic Field Laboratory, Tallahassee, FL 32310, USA*

The CD147 receptor plays an integral role in numerous diseases by stimulating the expression of several protein families and serving as the receptor for extracellular cyclophilins; however, neither CD147 nor its interactions with its cyclophilin ligands have been well characterized in solution. CD147 is a unique protein in that it can function both at the cell membrane and after being released from cells where it continues to retain activity. Thus, the CD147 receptor functions through at least two mechanisms that include both cyclophilin-independent and cyclophilin-dependent modes of action. In regard to CD147 cyclophilin-independent activity, CD147 homophilic interactions are thought to underlie its activity. In regard to CD147 cyclophilin-dependent activity, cyclophilin/CD147 interactions may represent a novel means of signaling since cyclophilins are also peptidyl–prolyl isomerases. However, direct evidence of catalysis has not been shown within the cyclophilin/CD147 complex. In this report, we have characterized the solution behavior of the two most prevalent CD147 extracellular isoforms through biochemical methods that include gel-filtration and native gel analysis as well as directly through multiple NMR methods. All methods indicate that the extracellular immunoglobulin-like domains are monomeric in solution and, thus, suggest that CD147 homophilic interactions *in vivo* are mediated through other partners. Additionally, using multiple NMR techniques, we have identified and characterized the cyclophilin target site on CD147 and have shown for the first time that CD147 is also a substrate of its primary cyclophilin enzyme ligand, cyclophilin A.

*Corresponding author. E-mail address: Elan.Eisenmesser@UCDenver.edu.

Current address: V. Yurchenko, Laboratory of Lymphocyte Signaling, Rockefeller University, New York, NY 10065, USA.

Abbreviations used: CypA, cyclophilin A; CypB, cyclophilin B; MMP, matrix metalloproteinase; RA, rheumatoid arthritis; HIV-1, human immunodeficiency virus type 1; Itk, interleukin-2 tyrosine kinase; TM, transmembrane; HSQC, heteronuclear single quantum coherence; NOESY, nuclear Overhauser enhancement spectroscopy; MCT, monocarboxylate transporter; TFA, trifluoroacetic acid; TROSY, transverse relaxation optimized spectroscopy.

[8]WR Wiley Environmental
Molecular Sciences Laboratory,
High Field NMR Facility,
Richland, WA 99532, USA

Received 23 March 2009;
received in revised form
21 May 2009;
accepted 28 May 2009
Available online
3 June 2009

Edited by M. F. Summers

Keywords: cyclophilin; CD147; extracellular matrix metalloproteinase inducer (EMMPRIN); isomerization; proline

Introduction

The cellular receptor CD147 (also known as extracellular matrix metalloproteinase inducer or EMMPRIN) is expressed in nearly every cell type including fibroblasts,[1] platelets,[2] and T-cells[3] where its biological roles include the regulation of multiple protein families. For example, CD147 stimulates the secretion of numerous matrix metalloproteinases (MMPs) that are responsible for the reconstruction of the extracellular matrix[4] and CD147 has been shown to stimulate secretion of several pro-inflammatory cytokines.[2] In cancer, CD147 overexpression underlies tumorigenesis and CD147-mediated stimulation of MMPs is a critical part of metastasis.[5,6] Expression levels of CD147 are so high during disease progression that CD147 has been termed a "biomarker" for prostate,[7] liver,[8] and gastric cancer.[5] Moreover, in several types of cancer cells, CD147 is released in various soluble forms where it continues to play an active role in stimulating MMP secretion in distal cells.[9–11] CD147 is also overexpressed in inflammatory disorders such as rheumatoid arthritis (RA) where CD147-mediated MMP secretion leads to the destruction of joint tissue.[12,13] While CD147 is thought to act as its own receptor, whereby either membrane-bound or soluble CD147 participate in homophilic interactions with membrane-bound CD147 to stimulate intracellular signaling[14,15] (Fig. 1, mechanism 1), a rapidly growing list of CD147 protein interactions has emerged over the last 5 years, suggesting that CD147-mediated signaling may be orchestrated by other proteins. Such protein interactions may include integrins,[16] syndecan-1,[17] and the recently identified enzyme ligands of CD147, the cyclophilin class of peptidyl–prolyl isomerases.[18]

Cyclophilins are ubiquitously expressed enzymes that catalyze isomerization of peptidyl–prolyl bonds and regulate a diverse array of protein functions. For example, analogous to methylation and phosphorylation, cyclophilin-mediated isomerization is thought to be the underlying regulatory phenomena of several signal transduction pathways.[19] Similar to their CD147 receptor, cyclophilins are highly expressed in multiple cancers[20] and inflammatory disorders such as RA.[21] In fact, it was within the synovial fluid of RA patients that the prototypical cyclophilin family member, cyclophilin A (CypA), was first identified as an extracellular protein.[22] Later studies showed that CD147 functions as a signaling receptor for extracellular CypA as well as another cyclophilin, cyclophilin B (CypB).[23,24] Extracellular cyclophilins exhibit cytokine-like properties and mediate numerous intracellular events through their interactions with the CD147 receptor[18,25] (Fig. 1, mechanism 2). For example, CypA displays potent chemotactic activity that is dependent on its interaction with CD147[24] and inhibition of the CypA/CD147 interaction greatly decreases migration of immune cells to the sites of inflammation in mouse models of such diseases as acute lung injury,[26] asthma,[27] and RA.[28] Moreover, while many viruses utilize host cell CypA for infection, including vesicular stomatitis virus,[29] vaccinia virus,[30] human immunodeficiency virus type 1 (HIV-1),[31] and severe acute respiratory syndrome (SARS),[32] a subset of these viruses has been shown to rely on host cell

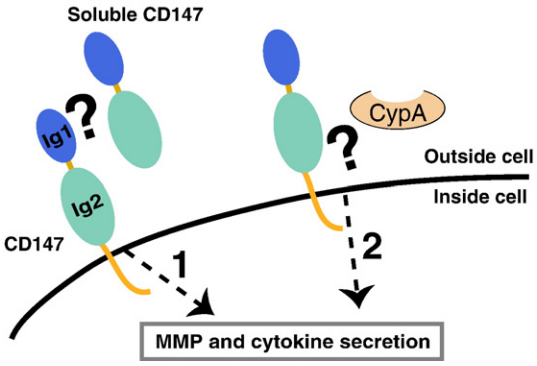

Fig. 1. CD147 functions through both cyclophilin-independent and cyclophilin-dependent mechanisms. Both mechanisms stimulate the secretion of MMPs and pro-inflammatory cytokines. These mechanisms include the following: Mechanism 1, CD147 homophilic interactions occur both between neighboring cells as well as soluble CD147 released by cells through several known mechanisms (see the text). Mechanism 2, extracellular cyclophilin enzymes target the CD147 receptor. CD147 Ig-like domains, Ig1 (blue) and Ig2 (green), are shown along with the predicted flexible regions (orange) and CypA (khaki).

CD147 as well. Specifically, in both HIV-1 and SARS, virus-associated CypA that is "hijacked" from a previous host cell and anchored within the viral membrane has been proposed to increase infection by targeting CD147 on a new host cell. In support of such a proposal, specifically blocking CypA/CD147 interactions inhibits infection in cell culture.[32,33] Therefore, understanding the molecular mechanisms of cyclophilin/CD147 interactions may have profound therapeutic value with respect to therapies for cancer, inflammation, and viral infection.

CD147 homophilic interactions and cyclophilin/CD147 interactions comprise the two dominant mechanisms that lead to CD147-mediated intracellular signaling and ultimately chemotactic response, MMP secretion, and cytokine secretion (Fig. 1), yet the molecular basis of such interactions remains unknown. Based on the X-ray crystal structure of the CD147 extracellular region, it was suggested that several crystal contacts persist in solution with subnanomolar affinity,[34] yet there is little biochemical or biophysical data to support such a conclusion. Furthermore, while cyclophilin/CD147 interactions may represent a newly discovered mechanism of signal transduction, whereby cyclophilin-mediated peptidyl–prolyl isomerization of CD147 on the outside of the cell results in a conformational rearrangement on the inside of the cell, direct evidence of such a catalytic mechanism is still absent. The only present support of a catalytic role of CypA in CD147-mediated signaling comes from the use of an active-site mutant, $CypA^{R55A}$, which was shown to exhibit little activity compared to wild-type CypA.[35] However, the affinity of this same mutant to its substrates is nearly an order of magnitude weaker than that of wild-type CypA,[36] and therefore, the only conclusion that can be drawn is that the interaction is mediated through the CypA active site. Thus, here, we have initiated solution studies to probe both the CD147 homophilic interactions and CD147 interactions with its enzyme ligand, CypA.

By utilizing multiple solution experiments that include nuclear magnetic resonance (NMR), we have discovered that the extracellular region of CD147 does not self-associate in the absence of another molecule and that CypA both binds and catalyzes a single site within CD147, Pro211. This residue is predicted to lie just outside of the extracellular membrane. Interestingly, CD147 Pro211 already exists in an inherent *cis*:*trans* equilibrium in the absence of CypA, yet CypA-mediated catalysis of this site leads to a higher rate of interconversion and likely a higher *cis* content within the active CypA/CD147 complex than in the uncatalyzed CD147 receptor alone. A similar pre-existing equilibrium has previously been observed for the only other two CypA protein substrates studied to date via NMR, that is, the HIV-1 capsid[37] and the interleukin-2 tyrosine kinase (Itk),[19] suggesting that an increase in the *cis* conformation of a bound substrate may be a general mechanism for CypA-mediated control of protein function. More specifically, our studies here suggest that CypA catalysis, which has been proposed to regulate a *cis*/*trans* "conformational switch" inside the cell,[19] may also perform a similar task to CD147 on the outside of the cell. Thus, CypA-mediated peptidyl–prolyl isomerization appears to regulate signal transduction at several levels. Our findings are the first to directly show that CD147 is a substrate of its extracellular ligand CypA and strongly suggest that CD147 homophilic interactions are mediated by another molecule such as a co-receptor.

Results

Assessing proper refolding of recombinant CD147 and probing CD147 oligomerization

Intracellularly expressed CD147 constructs in bacteria are initially unfolded due to improper disulfide formation but can be refolded *in vitro* to yield milligram quantities of highly soluble and biologically active proteins. The extracellular region of the dominant CD147 isoform (isoform 2, which is $CD147^{22–269}$) contains two Ig-like domains, herein called Ig1 (residues 22–103) and Ig2 (residues 105–205), and each contains two cysteine residues that form a single disulfide bond within each domain. The extracellular region of a less widely found CD147 isoform comprises only the Ig2 domain (isoform 3, which is $CD147^{94–269}$). The presence of these disulfide bonds was recently confirmed by the X-ray crystal structure of the CD147 extracellular region purified from a bacterial periplasmic expression system that relies on spontaneous folding within this oxidizing environment.[34] However, here we have discovered that both of these isoforms can be readily refolded in their entirety after intracellular bacterial expression to produce soluble proteins (both with and without the signal peptide sequence of residues 1–21, although these residues lead to soluble oligomers). While we can produce many soluble constructs of CD147 that represent different regions of the receptor via our *in vitro* refolding method (see Materials and Methods), CD147 constructs containing residues 215–229, which correspond to the hydrophobic transmembrane (TM) region, form large aggregates as assessed by size-exclusion chromatography (Fig. 2a, $CD147^{22–269}$). Removal of residues 205–229 that comprise both the membrane-proximal and TM region completely abrogates aggregation (Fig. 2a, $CD147^{22–269\Delta TM}$). Refolded CD147 constructs comprising the extracellular Ig-like domains were all found to elute as a single monomeric species on size exclusion and were therefore further analyzed by both SDS-PAGE denaturing gels and native gel analysis below.

Three CD147 constructs representing either the individual Ig-like domains alone, $CD147^{22–103}$ (Ig1) and $CD147^{94–205}$ (Ig2), as well as both domains, $CD147^{22–205}$ (Ig1 and Ig2), were used to probe both proper disulfide formation and the oligomeric properties of CD147. The single disulfide bond

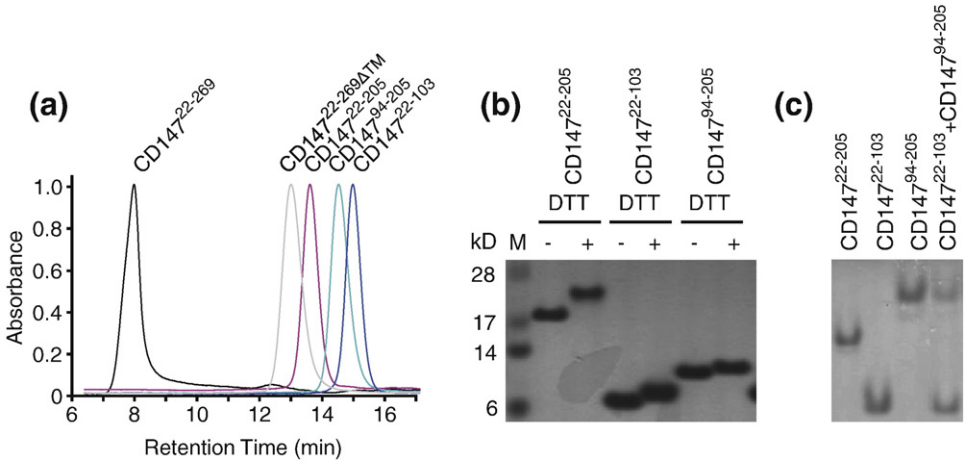

Fig. 2. Purified CD147 constructs exist as single monomeric species in solution in the absence of the TM region. (a) Size-exclusion chromatography of a subset of the constructs analyzed in this study and their retention volume upon loading 100 μl of 1 mg/ml of each sample onto an analytical Superose-12 column (column volume, 24 ml). Only constructs that contain the full TM domain, such as the full-length protein $CD147^{22–269}$, induce the formation of large oligomers, as shown by their elution at the void volume (~8 ml). The estimated molecular weights of $CD147^{94–205}$ and $CD147^{22–103}$ elute near the predicted molecular weights of a monomer, while both $CD147^{22–269\Delta TM}$ and $CD147^{22–205}$ elute higher due to their flexible regions and the flexible nature of the linker region between the two Ig-like domains. (b) Denaturing gel of CD147 constructs containing both domains ($CD147^{22–205}$), Ig1 ($CD147^{22–103}$), and Ig2 ($CD147^{94–205}$) in the absence and presence of DTT. Reduction of the single disulfide bond within each domain leads to slower migratory behavior. (c) Native gel of the same constructs confirms that all constructs run as a single species and that Ig1 and Ig2 do not interact (right lane).

within each extracellular CD147 domain was correctly formed by our refolding procedure as confirmed by SDS-PAGE denaturing gels where the presence of dithiothreitol (DTT) reduced each disulfide bond and led to a slower migrating species for all constructs (Fig. 2b). Furthermore, all extracellular CD147 constructs migrate as a single species on a native gel (Fig. 2c) and, together with the aforementioned size-exclusion data, suggest that with proper disulfide formation, each Ig-like domain neither self-associates nor interacts with the other Ig-like domain.

A final confirmation of proper refolding is shown in the biological activity of our recombinant CD147 (Fig. S1). Specifically, our refolded recombinant $CD147^{22–205}$ stimulates the release of two well-characterized pro-inflammatory cytokines in cell culture, TNF-α and IL-1β, providing the first evidence that glycosylation of CD147 is not required for cytokine stimulation as has recently been shown for MMP stimulation.[14] However, caution must be taken in assessing the activity of unglycosylated CD147 since the explicit role of CD147 glycosylation is still poorly understood. For example, the unglycosylated form of CD147 has been found to act as an antagonist of MMP induction in some contexts[38] and there is growing evidence that supports the notion that the degree of CD147 glycosylation *in vivo* regulates its activity.[39,40] Moreover, "differentially glycosylated" does not necessarily imply that CD147 is unglycosylated *in vivo* and, in fact, there is no evidence to suggest that the soluble CD147 forms released from cells are not glycosylated. Thus, future studies aimed at producing glycosylated CD147 from, for example, mammalian expression systems will allow for a rigorous comparative analysis to our unglycosylated forms probed here.

Considering that several recent reports have identified trace amounts of CD147 dimerization using one of the exact same constructs that we have begun characterizing here, namely, $CD147^{22–205}$, it is important to rationalize why we do not observe such a phenomena.[14,34] The most likely explanation for these observed differences is intermolecular disulfide bond formation. Specifically, the previous purification schemes of recombinant $CD147^{22–205}$ relied on spontaneous refolding in the oxidizing environment of the *Escherichia coli* periplasm and this likely leads to a small population of incorrectly folded protein, which would be susceptible to intermolecular disulfide formation. In contrast, our *in vitro* refolding procedure may simply be more efficient since we do not observe such dimers on SDS-PAGE or native gel analysis. However, such cross-linked dimers can still be observed within our protein preparations using Western blot analysis, indicating that even our purification procedure produces trace amounts of this cross-linked dimer, albeit at far lower relative concentrations to the monomeric species (Fig. S2). While we suspect that these dimers are simply a by-product of purification rather than a biologically relevant protein, it would be naïve to completely rule out a potential role of disulfide shuffling for CD147 homophilic interactions. However, receptor interactions that rely on disulfide shuffling require other protein interactions such as protein disulfide isomerase[41] and such interactions have not been identified for CD147. Regardless of such hypothetical interactions, our data indicate that the extracellular region of the

intact fully folded monomeric extracellular domains of CD147 do not self-associate in the absence of another mediator.

NMR solution studies of the CD147 Ig-like domains

While the extracellular domains of CD147 neither self-associate nor interact with each other under the concentrations used for native gels (i.e., low micromolar concentrations), receptors implicated in cellular adhesion, such as CD147, sometimes exhibit weak affinities. Since several reports have indicated that CD147 acts as its own receptor analogous to other cellular adhesion receptors,[42] such affinity could potentially be under the detection limit of our native gel analysis performed above. In contrast, NMR solution experiments can be used as particularly sensitive markers of such protein/protein interactions on multiple timescales and are therefore well suited to probe interactions with various affinities. For example, NMR titration experiments offer an obvious means of monitoring interactions that exhibit affinities on the order of the concentrations utilized (micromolar to millimolar concentrations). Additionally, NMR relaxation experiments provide the dynamic details of each residue and, thus, if the individual Ig-like domains of CD147 self-associate, then this may be detected at atomic resolution. To this end, we have completed the backbone resonance assignments of the extracellular regions of the two most prevalent CD147 isoforms $CD147^{22–205}$ (isoform 2 comprising both Ig1 and Ig2) and $CD147^{94–205}$ (isoform 3 comprising Ig2) in order to characterize CD147 solution properties and its potential interactions at atomic resolution (Supplementary Material, Tables S1 and S2 and BMRB accession numbers 16322 and 7433).

A comparison of the aforementioned X-ray crystal structure of $CD147^{22–205}$ with our NMR solution studies indicates that there are both similarities and differences between the crystal structure and the solution structure. In regard to the monomeric structure in solution, the secondary-structure propensities of $CD147^{22–205}$ were calculated from our resonance assignments using the program TALOS[43] and are largely consistent with that found in the crystal (Fig. S3). In other words, the monomeric structure in solution is highly similar to that in the crystal. The only major difference is that the resonances corresponding to residues 151–159, which comprise a short α-helix and part of β-strand "D" in the crystal, are not observed in solution.[34] This indicates that at least part of residues 151–159 undergo chemical exchange (i.e., conformational exchange between two different chemical environments) on the intermediate NMR timescale and, therefore, sample multiple conformations with exchange rates that are similar to the chemical shift differences between sampled states (i.e., intermediate exchange).

NMR spectra, NMR relaxation experiments, and NMR titration experiments all indicate that the intermolecular contacts observed in the crystal are not maintained in solution. The extracellular regions of both CD147 isoforms give rise to high-quality spectra and are shown here in the context of 2D ^{15}N-edited heteronuclear single quantum coherence (HSQC) spectra (Fig. 3). While the high dispersion is indicative of characteristically well-folded proteins, the relatively narrow linewidths observed in solution already provide evidence that the four proposed subnanomolar interactions in the crystal do not persist in solution (Fig. 3a and b, top right). R1 (longitudinal) and R2 (transverse) relaxation rates measured here define the correlation times of each amide and indicate that CD147 residues 22–101 (i.e., Ig1) and residues 105–205 (i.e., Ig2) are independently rotating domains within $CD147^{22–205}$ (Fig. 3a and b, bottom). The correlation time for each domain was calculated from all residues with R2/R1 ratios within one standard deviation using the equation described by Larsson *et al.*,[44] and the differences are immediately apparent in the raw data. For example, the average R2 rates are about 22 Hz for residues 22–101 and 35 Hz for residues 105–205, indicating that these domains exhibit markedly different tumbling times in solution. While these differing R2/R1 ratios are consistent with the two independently folded Ig-like domains found within the X-ray crystal structure,[34] the fact that these domains tumble with different correlation times provides evidence that the inter-domain interactions observed in the crystal are not maintained in solution. In other words, the CD147 Ig1 and Ig2 domains would be expected to exhibit the same correlation time if they self-associated in solution. To rule out the possibility of anisotropic rotation, correlation times for each of the individual domains were also calculated using the FAST-Modelfree (Facile Analysis and Statistical Testing for Modelfree) analysis[45] for each domain with an isotropic model and an anisotropic model. For the anisotropic model, each of the respective domains within the X-ray crystal structure was used. Correlation times calculated using an isotropic model were 11.8 and 14.1 ns for Ig1 and Ig2, respectively, and for an anisotropic model, the correlation time for Ig1 was found to increase slightly to 12.6 ns while the correlation time for Ig2 was the same as that of the isotropic model. Thus, regardless of rotational anisotropy, the major finding from these relaxation experiments is that the tumbling times of the two CD147 Ig-like domains in solution differ by at least 1.5 ns. Consistent with these findings, no chemical shift changes were observed upon a titration of ^{15}N-$CD147^{94–205}$ with stoichiometric amounts of $CD147^{22–103}$ (Fig. S4), thereby proving that these two domains do not interact as separate entities even weakly (i.e., $K_d \sim 1.0$ mM). Moreover, no concentration-dependent chemical shift changes are observed for $CD147^{22–205}$ that would be expected to occur if there was even a weaker self-association (i.e., $K_d > 1$ mM). Finally, the R2/R1-derived correlation times for each domain and the observed linewidths are completely consistent with

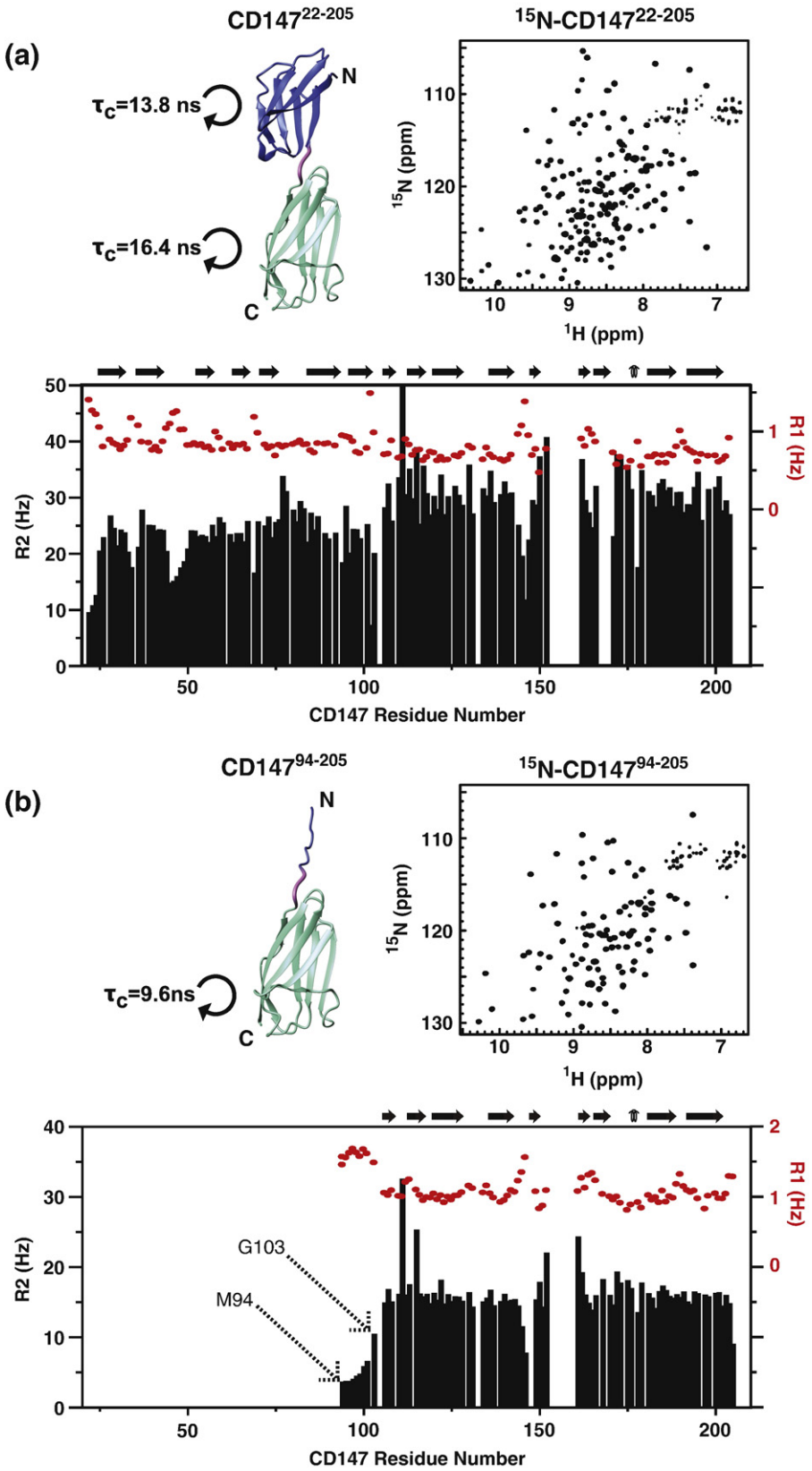

Fig. 3. NMR solution studies reveal that the CD147 Ig-like domains do not self-associate or interact with each other. The extracellular regions of the two major CD147 isoforms, (a) isoform 2 ($CD147^{22–205}$) and (b) isoform 3 ($CD147^{94–205}$), were characterized using NMR solution studies. The particular regions under study are shown using the X-ray crystal structure (Protein Data Bank accession code: 3B5H) with the corresponding ^{15}N-HSQC spectra and NMR relaxation data. Specifically, amide R1 (red dots) and R2 (black bars) relaxation rates were obtained for both CD147 constructs and used to calculate the correlation times. The extracted correlation times are shown adjacent to each Ig-like domain, Ig1 (blue) and Ig2 (green). Secondary-structure propensities are shown on top of each plot as calculated from our chemical shift assignments with the program TALOS.[43] All data were collected at 25 °C and 900 MHz.

monomeric proteins. Thus, the NMR solution data are consistent with the aforementioned native gels that also indicate that CD147 homophilic interactions do not occur through the extracellular region in the absence of another mediator.

Our NMR studies also offer important insight into residues 94–101 that comprise the N-terminal portion of the extracellular region of CD147 isoform3 (i.e., $CD147^{94–269}$). Namely, both resonance-based secondary-structure propensities and relaxation rates indicate that residues 94–101 form a β-strand only in the context of Ig1 but are disordered within the context of this shorter CD147 isoform 3 that only comprises Ig2 (Fig. 3b). With the use of our resonance assignments for this CD147 construct, no secondary-structure propensities were predicted by TALOS and the corresponding low R2 rates and high R1 rates are consistent with disordered residues (Fig. 3b, bottom).

Identification and initial characterization of the CypA target site of CD147

We have discovered that a region within CD147 exists in an inherent *cis*/*trans* equilibrium dictated by a central proline residue and that CypA both enhances the rate of this interconversion and likely alters the *cis*:*trans* ratio upon complex formation. Moreover, this preexisting equilibrium may be a general phenomenon for biological substrates of cyclophilins since an unusually high *cis* content has also been observed for other CypA protein substrates.[19,36,37] Several previous studies have suggested that CypA could target both CD147 Pro180[24] and Pro211,[46] yet cyclophilin binding to CD147 has only been investigated within the context of peptides.[46,47] Thus, we now provide the first direct evidence that shows that CypA exclusively targets CD147 Pro211, and not Pro180, in the context of the fully folded protein. Furthermore, CypA catalyzes peptidyl–prolyl isomerization of only this single Pro211 site. Our determination of the CD147 resonance assignments allows for the characterization in solution of this receptor with its enzyme ligand CypA that has itself previously been assigned in solution both free[48] and in the context of several substrates.[36,49]

NMR titration experiments were first conducted using ^{15}N-CypA with unlabeled CD147, and chemical shift changes were only observed for extracellular recombinant CD147 constructs that included the membrane-proximal region of CD147 residues 206–214. No interactions between CypA and the Ig-like domains of CD147 were detected using either $CD147^{94–205}$ or $CD147^{22–205}$ (data not shown), while identical chemical shift changes were observed

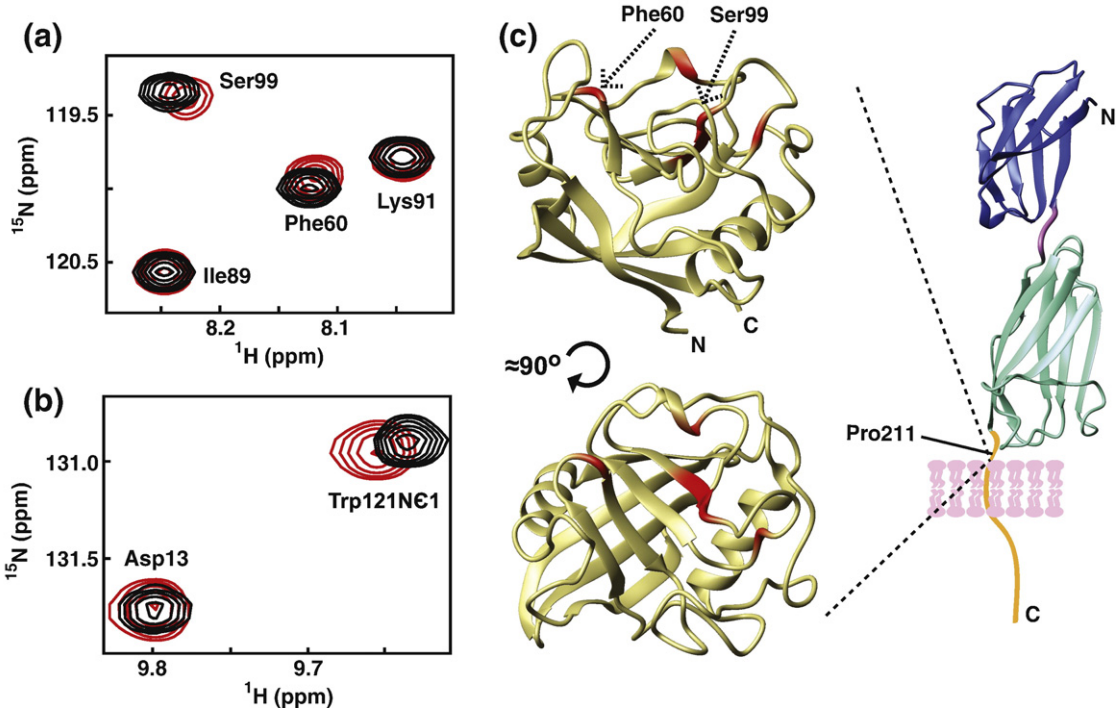

Fig. 4. CypA specifically engages CD147 through its active site. (a) ^{15}N-TROSY-HSQC spectra of 0.5 mM free ^{15}N-CypA (black) and in the presence of 1 mM $CD147^{22–214}$ (red) indicate that only the chemical environment of CypA active-site residues such as Ser99 and Phe60 are perturbed by the interaction. (b) Within these same spectra, ^{15}N-CypA $Trp121^{N\varepsilon 1}$ that is located in the short 3,10–α-helix adjacent to the active site also exhibits chemical shift perturbation in the presence of $CD147^{22–214}$. (c) Two views of the CypA residues that exhibit chemical shift perturbations upon addition of $CD147^{22–214}$ are shown, along with a cartoon extension of the Ig-like domains that contain the targeted Pro211. Residues are colored (red) onto our previously determined X-ray crystal structure of CypA (Protein Data Bank accession code: 1ZKT) if their respective chemical shift differences were greater than 0.06 ppm as defined by $\sqrt{(5\Delta\nu_{1H})^2 + (\Delta\nu_{15N})^2}$. Titrations were conducted at 25 °C and at 900 MHz.

for two constructs containing residues 206–214, $CD147^{94-214}$ and $CD147^{22-214}$ (Fig. 4a). These CD147 residues are predicted to lie at the surface of the extracellular TM region, and some of these residues may even lie within the membrane itself. However, both extracellular cyclophilin ligands of CD147, CypA and CypB, are known to readily traverse the membrane.[20] Upon titration of these latter CD147 comprising residues 206–214 to ^{15}N-CypA, both CypA amide residues (Fig. 4a) and the single CypA indole of Trp121 (Fig. 4b) were found to exhibit chemical shift changes that were all localized to the CypA active site (Fig. 4c, left). Thus, CypA specifically engages CD147 within residues 206–214 through its active site and there is only a single potential targeted residue, Pro211, within this region (Fig. 4c, right). Furthermore, only a single set of CypA resonances was observed during such titrations, indicating that exchange between the free and bound states is fast on the NMR chemical shift timescale and the affinity of these two proteins is relatively weak. Also in support of such a weak affinity of the CypA/CD147 complex, the measured chemical shift changes were linear over the titration range employed, indicating our inability to fully saturate all CypA binding sites (CD147 constructs were not stable beyond 1–2 mM). Our data therefore imply that the binding affinity of CypA/CD147 is weaker than the highest CD147 concentration used (i.e., K_d>1 mM since 1 mM was our final titration point) and is consistent with the relatively weak affinity cyclophilins have for most of their substrates.[50] Such weak affinity also explains the failure of previous pull-down experiments.[24] Thus, CypA targets CD147 within residues 207–214 specifically but with relatively weak affinity.

While the relative weak affinity of CypA for CD147 residues 206–214 does not allow for saturating concentrations necessary to accurately determine their binding affinity, we have used a peptide representing this region of interest as an alternative method. Specifically, we have estimated the affinity of CypA to CD147 residues 206–214 using a peptide, herein called the $CD147^{10mer}$ (sequence of 205-HLAALW**P**FLG-214), which corresponds to the CypA target site on CD147. The use of a representative peptide for this CD147 target site was warranted based on both R1 and R2 measurements, since this membrane-proximal region is highly flexible on the fast timescale (Fig. S5). In accord with previous studies that have suggested that the CypA/CD147 interaction is of relative weak affinity,

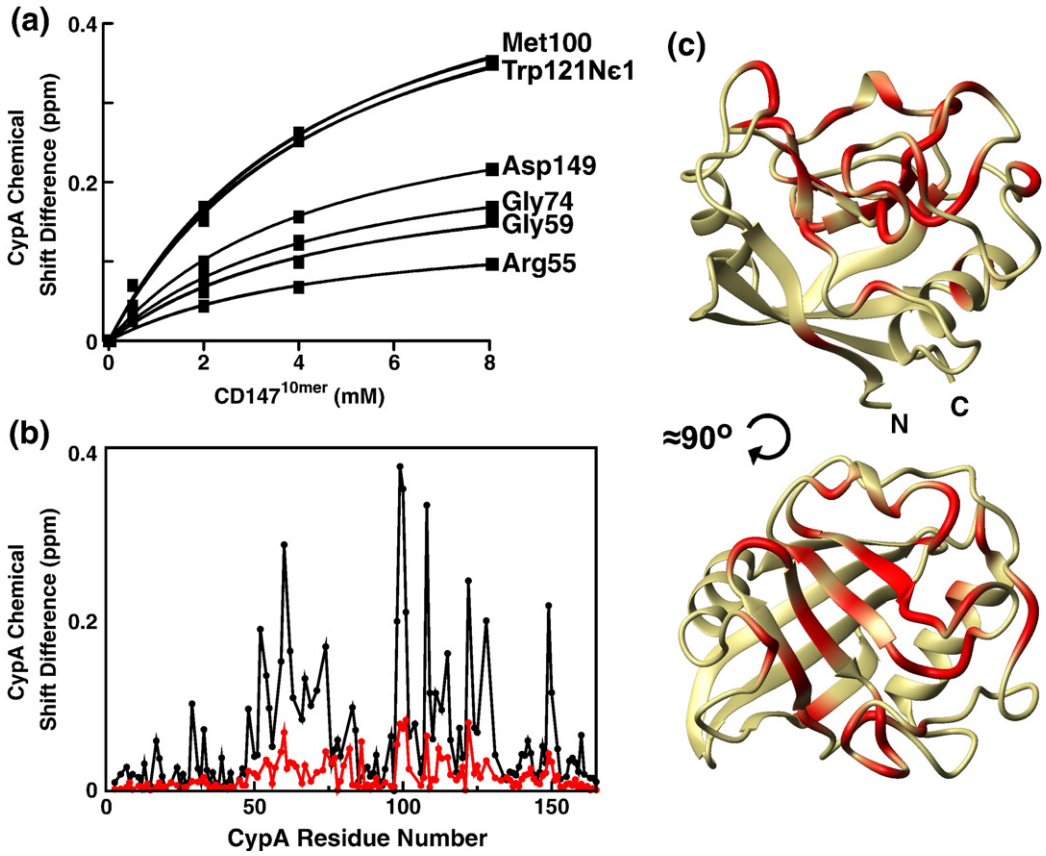

Fig. 5. Quantifying the binding interaction between CypA and CD147. (a) Binding isotherms are shown for both ^{15}N-CypA active-site amides and the single indole of the active-site Trp121 upon addition of a peptide that corresponds to CD147 residues 205–214, the $CD147^{10mer}$. A K_d of 4.2±0.2 mM was extracted from these fits. (b) Chemical shift changes of ^{15}N-CypA are compared upon titration of $CD147^{22-214}$ (1 mM, red) and the $CD147^{10mer}$ peptide (8 mM, black). (c) CypA chemical shift changes with the $CD147^{10mer}$ peptide are relegated to the active site as they are with the larger CD147 constructs. All chemical shift changes were calculated as in Fig. 4. Experiments were collected at 25 °C and at 900 MHz.

a K_d of 4.2±0.2 mM was calculated from the binding isotherms between ^{15}N-CypA and the CD147^{10mer} (Fig. 5a). Many more residues exhibit chemical shift changes using this peptide due to our ability to titrate to saturating conditions (Fig. 5b) and, as expected, these perturbations are still confined to the active site, confirming CypA specificity for this peptide (Fig. 5c).

Upon reversing the labeling scheme to monitor CypA-induced changes to ^{15}N-CD147$^{22–214}$, two sets of resonances were found for residues 207–214 corresponding to an inherent *cis*/*trans* conformational exchange of Pro211 (Fig. 6a and b, black spectra). Strikingly, a similar preexisting conformational equilibrium has been observed for the two CypA substrates studied to date, the HIV-1 capsid (HIV-1 CA)[36,37] and Itk.[19] In CD147, the mutation of this proline to an alanine, that is, CD147^{P211A}, probed in the context of either CD147$^{22–214}$ or CD147$^{94–214}$, resulted in only a single set of resonances (Fig. S6), confirming that proline isomerization is the underlying cause of this inherent conformational heterogeneity. Many of the resonances within CD147^{P211A} also overlapped with those resonances corresponding to the major conformation observed in the wild-type receptor, simultaneously confirming that the *trans* conformer dominates in the wild-type receptor and allowing us to assign the *cis* resonances. From the relative peak intensities in wild-type CD147, a *cis*:*trans* ratio of 33%:67% was calculated (i.e., 33% of CD147 Pro211 molecules are in the *cis* conformation), which is about twice the *cis* content as that of the HIV-1 CA[36] and very similar to that of Itk.[51] Thus, all three CypA protein substrates that have now been studied at the molecular level, that is, the HIV-1 CA, Itk,

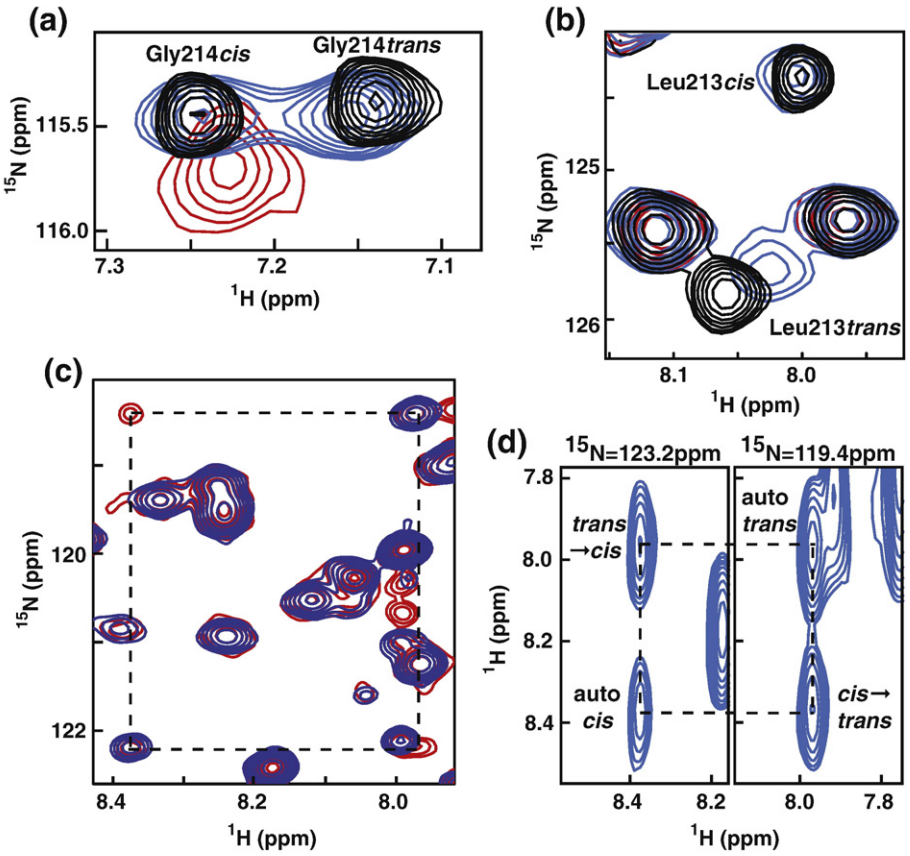

Fig. 6. CD147 is a substrate of CypA. (a) ^{15}N-TROSY-HSQC spectra of 0.5 mM free ^{15}N-CD147$^{94–214}$ (black) and in the presence of both 100 μM CypA (blue) and 1 mM CypA (red) show that upon titration of the enzyme, CD147 Gly214 amide *cis* and *trans* resonances converge. Thus, relative to the CypA-bound chemical shift difference between the CD147 Gly214 *cis* and *trans* conformations, the CypA induced conformational exchange rate is fast. (b) Several of the CypA-targeted CD147 residues, such as CD147 Leu213, exhibit severe linebroadening in the presence of substoichiometric concentrations of the enzyme and disappear under stoichiometric concentrations. Thus, relative to the CypA-bound chemical shift differences, the CypA-induced conformational exchange is on the intermediate timescale. (c) Using 0.5 mM ^{15}N-CD147$^{94–214}$, ZZ-exchange cross peaks are observed for residues 207–214 in the presence of catalytic concentrations of CypA. Shown here is the corresponding spectrum of the CD147 Phe212 amide with 0.05 mM CypA and a mixing time of 0 ms (dark blue) and 300 ms (red). (d) 3D-NOESY-HSQC of 0.5 mM ^{15}N-CD147$^{94–214}$ and 0.01 mM CypA utilizing a 150-ms mixing time also identifies exchange peaks for CD147 residues 207–214 as shown for Phe212. In the absence of CypA, no such cross peaks are observed for either ZZ-exchange or within 3D-NOESY-HSQC experiments, indicating a much slower uncatalyzed exchange between CD147 *cis* and *trans* conformations (data not shown). All experiments were conducted at 25 °C. Titrations were acquired at 900 MHz, and both ZZ-exchange and 3D-NOESY-experiments were acquired at 720 MHz.

and CD147, exhibit this intrinsic conformational equilibrium of the targeted proline with an unusually high *cis* content. Moreover, it is likely that enzyme-mediated catalysis alters these equilibriums (upon complex formation) as described below (see Discussion).

Evidence for CypA-mediated catalysis of CD147 was initially provided by a spectral comparison of free ^{15}N-CD147$^{94–214}$ to that titrated with stoichiometric concentrations of unlabeled CypA (Fig. 6a and b). The fact that two distinct sets of resonances are observed for free ^{15}N-CD147 residues 207–214 means that the intrinsic rate of peptidyl–prolyl isomerization is slow on the NMR timescale (<0.1 s^{-1}). In contrast, upon addition of stoichiometric concentrations of CypA, amide resonances within ^{15}N-CD147 residues 207–214 either converge or are so severely linebroadened that they disappear (Fig. 5a and b, respectively). This implies that in the presence of CypA, CD147 undergoes a conformational exchange on both the fast and the intermediate NMR timescale. In other words, the intrinsic interconversion of CD147 Pro211 is higher in the presence of CypA, and therefore, the conformational exchange of peptidyl–prolyl interconversion of Pro211 is enhanced by CypA-mediated catalysis. Those residues that converge undergo "fast exchange" and those residues that disappear undergo "intermediate exchange". However, this exchange is not simply relative to the bound

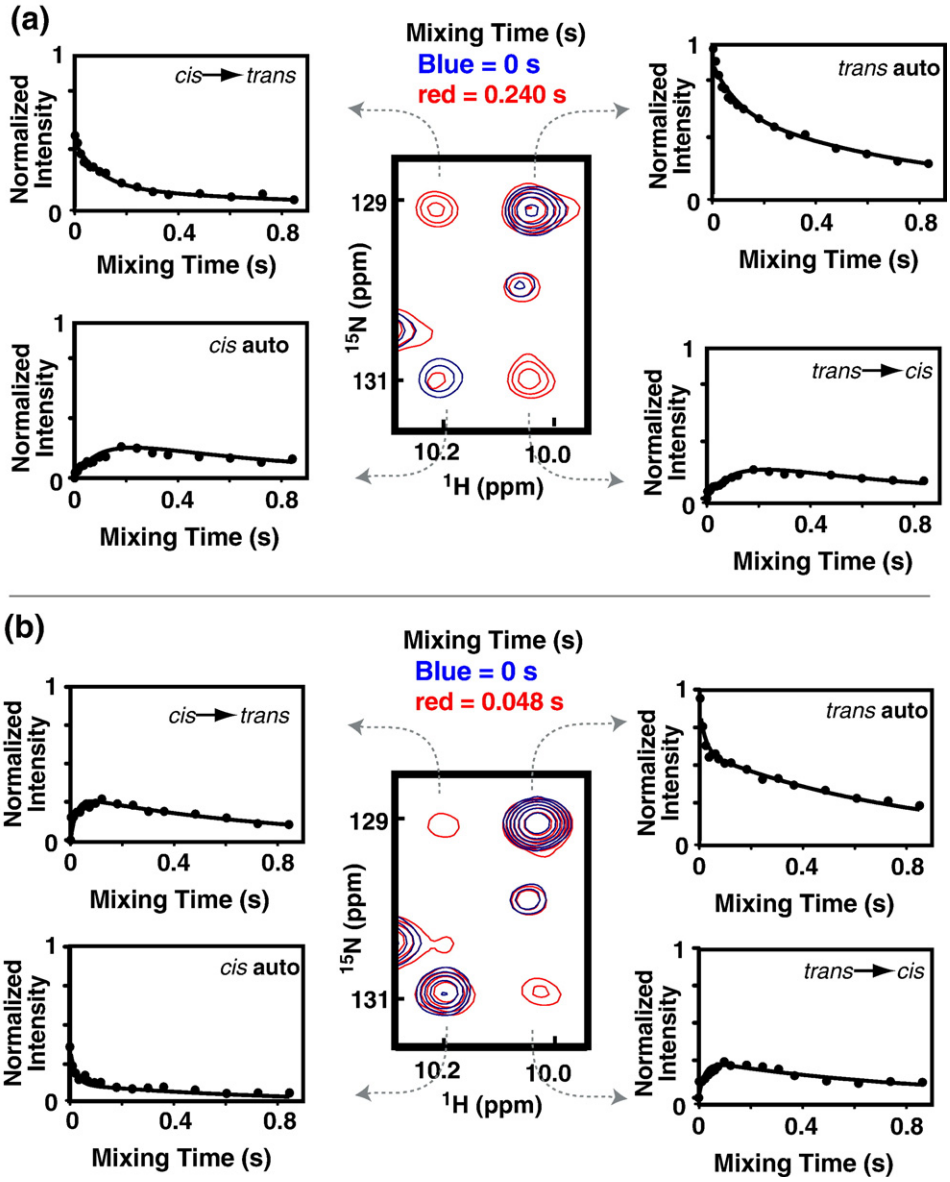

Fig. 7. Quantifying the catalytic rate of exchange for CypA-mediated isomerization of CD147. The apparent catalytic exchange rates in Table 1 were derived from ZZ-exchange experiments using [CD147$^{94–214}$]=0.5 mM and either (a) [CypA]=0.01 mM or (b) [CypA]=0.05 mM. The ZZ-exchange data along with the corresponding fits and two sample spectra from each experiment for CD147 Trp210$^{N\varepsilon 1}$ are shown. Intensities for each of the four resonances were fit simultaneously to Eqs. (1a), (1b), (1c), and (1d). Intensities were normalized to that of the highest intensity, that is, the *trans* resonance, at no mixing time.

chemical shift differences, since it also includes exchange to the free states due to the weak affinity of the complex. Finally, linebroadening of the active-site ^{15}N-CypA amide resonances is also observed above with the addition of unlabeled CD147 constructs, yet these do not completely disappear because it is the CypA side chains that likely make direct contact with the CD147 substrate.

Beyond the observed linebroadening of CD147 resonances in the presence of CypA, two additional NMR experiments provided direct experimental proof for CypA-mediated rate enhancement of CD147 peptidyl–prolyl isomerization. The appearance of exchange peaks between the corresponding ^{15}N-CD147 *cis* and *trans* resonances was observed in the presence of catalytic amounts of the enzyme for both "ZZ-exchange" experiments (Fig. 6c) and within standard 3D-nuclear Overhauser enhancement spectroscopy (NOESY) experiments (Fig. 6d). Such exchange peaks arise if the apparent rate of catalysis allows for transfer of magnetization between the two sampled states (i.e., *cis* and *trans*), occurring within the time frame of the experiment (i.e., the mixing times), and are only observed in the presence of CypA. Thus, the appearance of exchange peaks within both of these experiments indicates that CypA increases the intrinsically slow exchange of Pro211 and once again provides evidence that CD147 is a substrate of its CypA enzyme ligand.

Characterizing CypA-mediated catalysis of CD147

ZZ-exchange was used to determine the apparent catalytic exchange rate of CypA-mediated peptidyl–prolyl isomerization of CD147 Pro211, providing a quantitative analysis of the active CypA/CD147 complex (Fig. 7). Specifically, two ZZ-exchange experiments were collected using identical concentrations of 0.5 mM ^{15}N-CD147$^{94–214}$ but with two substoichiometric concentrations of the enzyme (i.e., catalytic concentrations) of 0.01 mM (Fig. 7a) and 0.05 mM (Fig. 7b) CypA. Under each condition, the apparent exchange rate (k_{ex}), which is the sum of the apparent *cis* → *trans* (i.e., k_{ct}) and *trans* → *cis* (i.e., k_{tc}) catalytic rates, was determined to quantify the rate enhancement of CypA-mediated catalysis (Table 1). Both the raw data and fits are shown for CD147 Trp210$^{N\varepsilon1}$ for all four peaks (i.e., both auto peaks and both exchange peaks), which is adjacent to the catalyzed CD147 Pro211. A verification of our sample preparations is shown by the fact that the maximum cross-peak intensities occur approximately 5-fold apart and corresponds to the 5-fold difference in enzyme concentrations (Fig. 7a and b spectra shown in center). For example, we observe maximum cross-peak intensities for CD147 exchange peaks at ~240 ms and ~48 ms for the 0.01 mM CypA sample and the 0.05 mM CypA sample, respectively. These data along with all non-overlapping amides within the CypA target site of CD147 residues 207–214 were used to calculate the apparent catalytic rate constants at each CypA concentration as shown in Table 1 (and for the residue-specific results, see Supplementary Material, Tables S3 and S4). Using our quantitative estimation of the K_d for the CypA/CD147 complex derived from our model peptide substrate above, 0.2% and 1.1% complex relative to the free ^{15}N-CD147$^{94–214}$ would exist for 0.01 and 0.05 mM CypA, respectively (see Supplementary Material, Section 2). Thus, extrapolating these apparent exchange rates (Table 1) to the fully bound complex gives approximately 4000–4800 s^{-1} for CypA-mediated interconversion of CD147 at 25 °C. While this is only a rough approximation of the CypA-mediated exchange rate, it is clear that CypA provides a significant rate enhancement relative to the uncatalyzed *cis*/*trans* exchange rate of peptidyl–prolyl isomerization that is less than 0.1 s^{-1}.[52] However, this rate enhancement is less than that in our previous study of a model peptide substrate measured at the same temperature.[49] A possible explanation for this lower catalytic rate is that CD147 has a bulky Trp residue preceding the catalyzed CD147 Pro211 (i.e., CD147 Trp210-Pro211) that likely slows the interconversion rate relative to the model peptide substrates. In fact, in a study conducted nearly two decades ago with various amino acid substitutions preceding the catalyzed Pro, the authors found that the Trp-Pro sequence exhibited the slowest k_{ct} rate for human CypA.[53] In conclusion, CypA catalysis serves to increase the uncatalyzed rate of interconversion by at least several orders of magnitude.

Table 1. Apparent catalytic exchange rates of CypA-mediated interconversion of CD147 residues 207–214 determined from ZZ-exchange

[CypA]	k_{ex} (s^{-1})	Fits used
0.01 mM	9.6±3.5	24
0.05 mM	44.3±8.1	20

Identical concentrations of 0.5 mM ^{15}N-CD147$^{94–214}$ were used with the listed concentrations of CypA, and the apparent catalytic exchange rates were derived from ZZ-exchange data using Eqs. (1a), (1b), (1c), and (1d) (see Materials and Methods). All four non-overlapping peaks within ZZ-exchange spectra (both *cis* and *trans* auto peaks and both exchange peaks) were fit simultaneously for each amide within CD147 residues 207–214 and Trp210$^{N\varepsilon1}$, and the average of these with standard deviations are reported here (see Supplementary Material, Tables S3 and S4 for independently calculated parameters).

Discussion

The extracellular region of CD147 does not self-associate

We have directly characterized the extracellular regions of the two most dominant CD147 isoforms, isoform 2 (CD147$^{22–269}$) and isoform 3 (CD147$^{94–269}$), using multiple solution techniques and have shown that neither self-associate in the absence of a mediator. Only single monomeric species were

detected for all CD147 constructs that correspond to these extracellular regions as confirmed by gel-filtration analysis, native gel analysis, and multiple NMR solution studies. In regard to the monomeric species, secondary-structure predictions based on our NMR resonance assignments are largely consistent with the X-ray crystal structure of the extracellular region of isoform 2, $CD147^{22-205}$, thereby confirming that the solution structure of the monomer is similar to that within the crystal. The only noted difference is that resonances corresponding to CD147 residues 151–159 are not observed in solution, and thus, this region likely undergoes a conformational exchange within the intermediate timescale (relative to the chemical shift differences between sampled conformations). Interestingly, this same region contains one of the three potential N-linked glycosylation sites (Asn152) and implies that inherent flexibility may be important for function. However, there are likely no contacts between the Ig-like domains and no preferred orientation relative to each other as observed within the recently solved X-ray crystal structure of $CD147^{22-205}$.[34] This conclusion is drawn from several experiments conducted here that indicate that the Ig-like domains themselves do not interact. Specifically, native gel analysis shows that both CD147 Ig1 and Ig2 domains exhibit the same migration patterns when combined as they do separately. Furthermore, in the context of the larger CD147 isoform 2, NMR relaxation experiments indicate that these domains exhibit very different correlation times in solution and, therefore, most likely tumble independently. No chemical shifts are observed within ^{15}N-HSQC experiments upon labeling one domain and titration of the other domain, confirming that the Ig-like domains do not interact as separate entities. Thus, our data provide direct evidence of free rotation around the short linker region between these two Ig-like domains (i.e., CD147 residues 103–105 that comprise the sequence Gly-Pro-Pro, respectively). Finally, we have, for the first time, characterized the solution properties of the extracellular region of the second most abundant CD147 isoform, isoform 3 (i.e., $CD147^{94-269}$). Here, we have found that the N-terminal residues 94–104 of isoform 3 are disordered as compared to the formation of a β-strand in the context of the Ig1 domain within the larger CD147 isoform 2.

Although the conclusions of several recent reports have suggested that a fraction of recombinant CD147 self-associates in solution,[14,34] there has been no direct proof that such an interaction occurs without mediation by another molecule *in vivo* (i.e., co-receptors or small molecules). In fact, much of these prior data are in agreement with our findings in this study. For example, there is a major contradiction between the data and the conclusions found within the recently published X-ray crystal structure of $CD147^{22-205}$.[34] Namely, these authors have suggested that the four interaction surfaces observed in the crystal give rise to highly favorable interactions with computationally calculated ΔG values ranging from −16 to −20 kcal/mol (i.e., subnanomolar K_d affinities). However, these same authors experimentally show that at mg/ml concentrations of CD147, only a small fraction forms dimers on a native gel, which should all be oligomers if any of their four calculated crystal contacts were truly of submicromolar affinity. Another contradiction in the literature is that the observed dimeric interactions of the extracellular region observed within native gels are abrogated in the presence of reducing agents, prompting some to conclude that this is due to protein unfolding caused by disulfide reduction.[14] However, a similar phenomenon is also observed within denaturing gels, suggesting that the dimers observed are simply intermolecular disulfides formed as a by-product of recombinant protein purification. Moreover, analogous to our findings, other groups have had difficulty in measuring CD147 self-association through its Ig1 and Ig2 domains.[54] Thus, CD147 oligomerization may be a far more complicated process than previously thought and likely involves mediation by other molecules such as a co-receptor to induce signaling (Fig. 8a).

While the current focus of our laboratory is to identify mediators of CD147 homophilic interac-

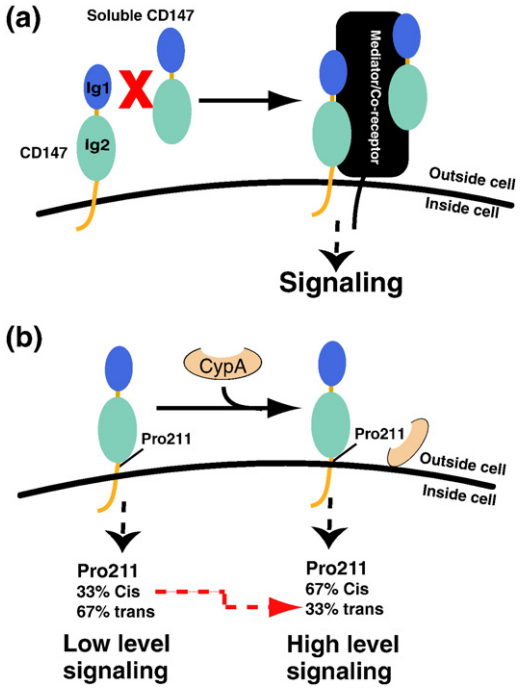

Fig. 8. Models for both the cyclophilin-independent and cyclophilin-dependent mechanisms of CD147 activity. (a) Based on our findings here that have shown that the extracellular region of CD147 does not self-associate, CD147 homophilic interactions are likely mediated by other molecules that potentially include TM proteins (i.e., co-receptors). (b) The direct observation of CypA-mediated isomerization of Pro211 suggests a mechanism whereby CypA may alter the inherent *cis:trans* equilibrium of CD147 Pro211. The inherent *cis:trans* ratio of CD147 Pro211 was calculated from the relative peak intensities of the amides of residues 207–214 within ^{15}N-HSQC spectra, and the *cis:trans* ratio in the active complex is based on previous studies with a model peptide substrate.[55] Colors are as defined in Fig. 1.

tions, it is important to begin addressing likely candidates since CD147 is a high profile player in the progression of many diseases. CD147 oligomerization in cell culture and *in vivo* may be modulated by small molecules as shown, for example, for cadherin dimerization that is modulated by calcium[56] or fibroblast growth factor receptor interactions that are mediated by heparins.[57] Thus far, we have not been able to identify such small-molecule interactions that affect CD147 self-association (data not shown), yet many other potential candidates that regulate CD147 homophilic interactions include membrane proteins such as monocarboxylate transporters (MCTs), syndecans, and integrins.[42] For example, an elegant fluorescent energy transfer study has revealed a 2:1 interaction between MCT-1 and CD147.[58] However, MCT-1 is predicted to have only short extracellular loops; thus, this TM protein seems an unlikely candidate for mediating homophilic interactions between cells. We have recombinantly expressed the entire extracellular region of syndecan-1, a well-known heparan sulfate proteoglycan that has recently been shown to co-localize with CD147 in cell lysates.[17] While we have discovered that syndecan-1 is primarily an unfolded protein, as expected from its primary sequence (i.e., within its 283 residues, there are 33 threonines, 30 glycines, and 25 prolines), it does not interact with the extracellular region of CD147 (Fig. S7). This may suggest that specifically attached glycans or the TM domains of CD147 and syndecan-1 modulate their interactions, and thus, probing such interactions biophysically awaits mammalian expression systems that produce full-length glycoproteins with relatively high yields.

CypA-mediated catalysis of CD147 likely represents a novel mode of intracellular signaling

While extracellular cyclophilins stimulate several intracellular signaling events through their CD147 receptor, the underlying mechanism has remained unclear. A direct interaction between cyclophilins and CD147 has been shown to occur both through yeast two-hybrid assays[24] and through the use of specific antibodies that block these cyclophilin/CD147 interactions.[23] Here, we have initiated studies that have allowed us to directly monitor the CypA/CD147 interaction in aqueous buffer during catalysis. Such studies are made possible due to the reversible nature of the cyclophilin-mediated reaction and serve as an important first step in understanding the link between peptidyl–prolyl isomerization on the outside of the cell and intracellular signaling. While both CypA and CypB have been shown to serve as the extracellular ligands of CD147, CypA is a more abundant protein and, thus, has been the focus of our studies here. Moreover, although NMR is a powerful technique that can reveal the atomic resolution details of molecular interactions, it is particularly useful in probing cyclophilin interactions that are of moderate to weak affinity.[50] Many weak but biologically important interactions occur in nature, which include adhesion proteins that exhibit micromolar affinities[59] and alcohols that exhibit millimolar affinities.[60] Thus, the high sensitivity of NMR to detect weak interactions was the initial impetus behind employing NMR methods to study the CypA/CD147 interactions at atomic resolution in solution.

Using NMR solution studies, we have shown that CypA both binds and catalyzes CD147 Pro211, a site predicted to lie on the outside of the cell and adjacent to the TM region of the receptor. Interestingly, this membrane-proximal region of CD147 residues 207–214 already exists in its free form in a *cis*:*trans* equilibrium characterized by an unusually high *cis* content of 33% (Fig. 8b, left). However, this uncatalyzed *cis*/*trans* isomerization is very slow, as evidenced by our observation of both sampled *cis* and *trans* resonances for all residues within this region of CD147. Upon addition of stoichiometric concentrations of CypA, ^{15}N-HSQC spectra collected on the active CypA/CD147 complex showed both the collapse of several *cis* and *trans* resonances and severe linebroadening for others, suggesting that a conformational exchange event occurs within the active CypA/CD147 complex (i.e., catalysis). Further proof of catalysis came from several NMR experiments collected under substoichiometric conditions, which unambiguously confirmed that CypA catalyzes CD147 Pro211. Namely, the appearance of exchange peaks in the both ZZ-exchange and 3D-NOESY experiments verifies a CypA-induced rate enhancement of the inherently slow *cis*/*trans* equilibrium of CD147 residues 207–214 and, therefore, provides direct evidence of CypA-mediated catalysis of its CD147 receptor. A quantitative analysis of our ZZ-exchange data reveals that the catalysis may be only slightly slower than that of nonnatural substrates previously studied, a finding reflective of the bulky CD147 Trp210 residue preceding the targeted Pro211.

Our confirmation that CD147 is a substrate of its CypA enzyme ligand along with several previous reports suggests an underlying mechanism for CypA-mediated signaling through the CD147 receptor (Fig. 8b, right). Specifically, this interaction likely encompasses a "conformational switch" responsible for regulating downstream signaling, whereby the relative *cis*:*trans* ratio of free CD147 Pro211 is increased by way of its CypA interaction. Both crystallography and NMR studies support such a model. For example, co-crystal complexes of CypA with various substrates are largely found in the *cis* conformation,[61,62] indicating that the relative affinity for the *cis* conformer is higher than that of the *trans* conformer. Based on such evidence, the *trans* → *cis* catalytic rate of CypA has been proposed to be higher than the *cis* → *trans* catalytic rate,[62] and thus, the relative *cis* population of CD147 within the catalyzed enzyme complex would be higher than that in the free state of CD147. Previous NMR studies that measured linebroadening of a model peptide substrate in the context of substoichiometric amounts of CypA have suggested that the relative *cis* population on the enzyme is higher than that of

the *trans* population.[55] Finally, previous NMR studies that measured CypA dynamics with saturating concentrations of the same model peptide were also consistent with a higher bound *cis* population.[63] Thus, for CD147, this would culminate in a reversal of the relative *cis*:*trans* populations upon CypA catalysis (Fig. 8b). Interestingly, a similar conformational switch mediated by CypA within the inside of the cell has also been proposed to regulate signaling.[19] Specifically, the SH2 domain of Itk also exists in an inherently slow interconverting *cis*/*trans* equilibrium dictated by a central proline residue and it is the *trans* conformation that binds a phosphotyrosine target peptide approximately 4-fold tighter than the *cis* conformation. Since this proline residue of Itk is also a substrate target of CypA, it seems possible that intracellular CypA mediates a similar regulatory phenomenon that we have proposed for CD147. In conclusion, CypA catalysis may regulate a conformational switch both inside and outside of the cell by way of increasing the relative *cis*:*trans* ratio of its substrates in the bound complexes (Fig. 8b).

By characterizing the active CypA/CD147 complex here, our studies represent an important step in unraveling the details of peptidyl–prolyl isomerization and the signaling events that follow, yet future work must now address these downstream interactions. Owing to the complex nature of CD147 interactions and its association with multi-protein complexes, at this point, we can only speculate as to how CypA-mediated catalysis may regulate intracellular signaling. For example, while it is clear that cyclophilin/CD147 interactions promote intracellular signaling events, recent data suggest that the intracellular C-terminal region of CD147 is not important for signaling.[64] Thus, analogous to the case of Itk where the conformation of a proline residue dictates its affinity for other proteins, the conformation of CD147 Pro211 may also dictate its affinity for a signaling-competent complex. Unfortunately, identifying such a complex (or complexes) is required to further address both the dynamic and structural changes that ensue upon CypA-mediated catalysis. Finally, although the CD147 Pro211 target site of CypA is predicted to lie outside of the TM and we have found that the inherent *cis*:*trans* equilibrium of CD147 is maintained in several different solvents (data not shown), we do not yet know how other protein interactions may alter this equilibrium. Thus, it will be critical to re-evaluate this equilibrium in the context of other protein interactions that will be identified in the future and then address how CypA-mediated catalysis alters such interactions.

Materials and Methods

Protein expression, refolding, and purification

In general, unlabeled proteins were produced in LB broth while labeled proteins were produced in M9 minimal media supplemented with required combinations of ^{15}N-ammonium chloride, ^{13}C-glucose, and 99% D_2O for NMR studies. All proteins were expressed in BL21 (DE3) cells, grown at 37 °C, and protein expression was induced using 0.1 mM isopropyl β,D-thiogalactopyranoside at an optical density of approximately 0.6 (600 nm). CypA was purified as previously described[49,63] while both CD147 and the extracellular region of syndecan-1 were purified as described below. Unless otherwise noted, all columns and resins were used on an AKTA FPLC purchased from GE Healthcare.

For CD147, all constructs were PCR-amplified from the previously described vectors[24] and ligated into the pET15b vector (EMD Biosciences, Inc., San Diego, CA) using NdeI and BamHI. All primers contained the appropriate restriction sites with six base-pair overhangs for cleavage prior to ligation. All CD147 proteins were refolded at 4 °C as follows. For a typical 2-L growth, cells were lysed via sonication in 35 ml of 100 mM Tris, pH 7.5, 0.5 M NaCl, and 1 mM ethylenediaminetetraacetic acid, centrifuged at 12,000*g* in a Sorvall SS-34 rotor (Sorvall, Asheville, NC), and the insoluble fraction was collected. The insoluble fraction was sonicated to homogeneity in 35 ml of denaturation buffer (5 M guanidine, 100 mM Tris, pH 7.5, 100 mM NaCl, and 2-mercaptoethanol), centrifuged again, and dialyzed into refolding buffer (1 M arginine, 100 mM Tris, pH 7.5, and 100 mM NaCl) for 48 h. Samples were subsequently dialyzed into 100 mM Tris, pH 7.5, and 300 mM NaCl for at least 12 h and centrifuged to remove any precipitation. The soluble refolded proteins were then further dialyzed into 50 mM $NaPO_4$, pH 7.5, 0.5 M NaCl, and 10 mM imidazole for purification via Ni Sepharose equilibrated in the same buffer and eluted in the same buffer supplemented with 0.4 M imidazole. Eluted proteins were cleaved overnight with thrombin; purified via a pre-packed S-100 size-exclusion column equilibrated with 50 mM $NaPO_4$, pH 6.5, 150 mM NaCl, and 50 mM imidazole; and then applied to a 1-ml benzamidine column in the same buffer to remove residual thrombin.

For syndecan-1, the extracellular region that corresponds to residues 23–251 was PCR-amplified from the commercially available plasmid (Open Biosystems, Huntsville, AL) and ligated into the pET15b vector (EMD Biosciences, Inc.) using NdeI and BamHI sites. Primers contained the appropriate restriction sites for cleavage prior to ligation. While there was no measurable expression of this pET15b-syndecan-1 from this constructed vector, subsequent insertion of streptococcal protein G (GB1) led to high protein expression. This was accomplished by PCR amplification of the 56-residue GB1 encoding region (vector described below) with NdeI restriction sites both 5′ and 3′ and subsequent insertion into the single NdeI-digested pET15b–syndecan-1 plasmid. Upon confirming that the GB1 sequence was inserted correctly, all further syndecan-1 purifications utilized this pET15b–GB1–syndecan-1 fusion that was entirely found in the soluble expressed fraction both before and after thrombin cleavage that released syndecan-1 residues 23–251 (with an N-terminal Gly-Ser). For a typical 2-L growth, cell pellets were lysed with 35 ml of 50 mM $NaPO_4$, pH 7.5, 0.5 M NaCl, and 10 mM imidazole and applied directly to a Ni Sepharose column in the same buffer. All subsequent purification steps were identical with that of the CD147 proteins described above.

Peptide expression and purification

A novel protocol for recombinant peptide production was employed to produce a peptide corresponding to CD147 residues 205–214, $CD147^{10mer}$. Unless otherwise

noted, all columns and resins were used on an AKTA FPLC purchased from GE Healthcare. Using standard PCR amplification, we constructed a PCR product with a 6×His, a thrombin site, and then the sequence of CD147 205–214 (HLAALWPFLG). A 5′ BamHI site and a 3′ EcoRI site were also included, and the PCR product was digested with the appropriate enzymes. Ligation of this PCR product into the pET30b vector that encoded GB1 (a kind gift from Gerhard Wagner, Harvard University) produced a vector encoding GB1 followed by our peptide of interest. This GB1–peptide fusion protein was expressed in BL21 (DE3) cells in LB broth supplemented with kanamycin. Cells were lysed in 50 mM $NaPO_4$, pH 7.5, 0.5 M NaCl, and 10 mM imidazole and then purified via a Ni Sepharose column equilibrated in the same buffer. The peptide was cleaved from this purified fusion with thrombin at room temperature for 12 h, leaving an N-terminal Gly-Ser followed by the CD147 residues 205–214 and then reapplied to Ni Sepharose resin in a gravity flow column. The pH of the eluted sample was decreased to 2 with trifluoroacetic acid (TFA) and then applied to a reversed-phase column (Agilent, Zorbax SB300, 9.6 mm×25 cm) using an HPLC (Agilent Technologies, Inc., Santa Clara, CA) equilibrated in 0.2% TFA/water and 0.18% TFA/acetonitrile solvent system. Finally, fractions containing the peptide were verified by analytical HPLC (Agilent, Zorbax SB300, 4.6 mm×15 cm) and mass spectrometry, pooled, and lyophilized for further use.

Analytical size-exclusion chromatography, gel electrophoresis, and Western blot analysis

Approximately 1 mg of the indicated CD147 purified proteins was applied to an analytical Superose-12 column (column volume, ~24 ml) that was equilibrated in the same buffer utilized for most NMR experiments (50 mM $NaPO_4$, pH 6.5, 150 mM NaCl, and 50 mM imidazole). Protein samples for SDS-PAGE contained 10 μl of 0.02 mM protein either with or without DTT, and the same concentrations of protein were used for native PAGE analysis. For Western blot analysis, SDS-PAGE gel electrophoresis of 10 μl of 0.02 mM recombinant $CD147^{22–205}$ was performed in the absence and presence of 1 mM DTT and then boiled for 5 min. The gel was transferred to an Immobilon PVDF membrane and blotted with 1:1000 Human Monoclonal EMMPRIN (R&D Systems, Minneapolis, MN) followed by 1:3000 anti-mouse horseradish peroxidase (Cell Signaling Technology, Danvers, MA). Protein band detection was performed with the ECL Chemiluminescence Detection Kit (Perkin Elmer, Waltham, MA) at three different exposure times (10, 30, and 60 s).

NMR sample preparation, spectroscopy, and data analysis

All NMR spectra were collected at 25 °C on a Varian 600 -, 720- , 800-, or 900-MHz spectrometer in 50 mM $NaPO_4$, pH 6.5, 150 mM NaCl, and 50 mM imidazole supplemented with 7% D_2O. There were only modest changes to the resonance positions with imidazole present (data not shown), yet imidazole did increase the lifetime of each sample slightly and, thus, was maintained in all samples. Samples utilized for assignment purposes contained 0.5–1 mM protein, while all samples utilized for titration purposes contained 0.5 mM protein with the indicated final concentration of the titrant. All spectra were processed using NMRPipe software[65] and analyzed using CCPNmr software.[66] Unless otherwise noted, all pulse sequences were obtained from standard Varian Biopack libraries. Transverse relaxation optimized spectroscopy (i.e., TROSY-based) HSQC experiments were used only when noted.

The backbone assignments of several CD147 constructs that included $CD147^{22–205}$ and $CD147^{94–205}$ as well as constructs containing the CypA target of CD147 Pro211, $CD147^{22–214}$, and $CD147^{94–214}$ were determined. Standard multidimensional NMR experiments that included an HNCACB and CBCA(CO)NH for each construct were used, while both a 3D-^{15}N-NOESY and a 3D-^{15}N-TOCSY (total correlated spectroscopy) were useful in confirming each spin system.[67] Our resonance assignments that were stored within the CCPNmr database were used to calculate secondary-structure propensities using the program TALOS.[43]

For relaxation experiments, standard R1 and R2 relaxation experiments were applied with recycle delays of 2.5 s at 900 MHz. Relaxation delays for R1 experiments were 0.01, 0.1, 0.3, 0.5, 0.7, 0.9, and 1 s, and relaxation delays for R2 experiments were 10, 30, 50, 70, and 90 ms. While compensating pulses prior to the recycle delay were utilized for R2 measurements to account for potential sample heating, all relaxation experiments were arrayed within a single experiment to also account for any potential field inhomogeneities. Correlation times for each amide were calculated using R2/R1 ratios as described in Larsson *et al.*[44] and correlation times for each domain using all R2/R1 ratios within one standard deviation of the mean. Correlation times for each domain were calculated using FAST-Modelfree employed Modelfree version 4.[45] Since calculations using Modelfree have recently been shown to become trapped in local minima,[68] a range in initial correlation times from 11 to 18 ns was used with 1-ns increments. While most calculations converged to the reported values and local minima were readily excluded due to large chi-squared values. In-house scripts that combined both NMRPipe and Gnuplot software were used to fit all relaxation rates using peak heights.

For ZZ-exchange experiments, the pulse scheme of Farrow *et al.* was employed with a selective adiabatic CHIRP pulse applied in the center of the mixing period for water suppression.[69] Two data sets were collected at 720 MHz on two samples with either 0.01 or 0.05 mM CypA and both containing 0.5 mM ^{15}N-$CD147^{94–214}$ at 25 °C and analyzed as previously described to calculate the apparent *cis*/*trans* exchange rate (k_{ex}).[36,70,71] Briefly, 14 mixing times (τ_m) were acquired for each of these two data sets ranging from 0 to 840 ms, and R1 relaxation rates used in fitting these data, that is, R1 for *cis* ($R1_c$) and R1 for *trans* ($R1_t$), were collected directly on these samples. Equations (1a), (1b), (1c), and (1d) were used to simultaneously fit the auto *trans* peak (I_{tt}), the auto *cis* peak (I_{cc}), the *trans*→*cis* exchange peak (I_{tc}) and the *cis*→*trans* exchange peak (I_{ct}), respectively, as a function of τ_m. $I_{tt}(0)$ and $I_{cc}(0)$ are the initial intensities of the *trans* and *cis* auto peaks, respectively, $a_{11}=R1_t+k_{tc}$, $a_{22}=R1_c+k_{ct}$, $a_{21}=-k_{tc}$, and $a_{12}=-k_{ct}$. Finally, under these conditions, k_{tc} and k_{ct} can be recast as a function of their free K_{eq} ($P_{cis}/P_{trans}=0.33/0.67$), and thus, $k_{tc}=0.33k_{ex}$ and $k_{ct}=0.67k_{ex}$.

$$I_{tt}(\tau_m) = I_{tt}(0)(-(\lambda_2 - a_{11})\exp(-\lambda_1\tau_m) + (\lambda_1 - a_{11})\exp(-\lambda_2\tau_m))/(\lambda_1 - \lambda_2) \quad (1a)$$

$$I_{cc}(\tau_m) = I_{cc}(0)(-(\lambda_2 - a_{22})\exp(-\lambda_1\tau_m) + (\lambda_1 - a_{22})\exp(-\lambda_2\tau_m))/(\lambda_1 - \lambda_2) \quad (1b)$$

$$I_{tc}(\tau_m) = I_{tt}(0)(a_{21}\exp(-\lambda_1\tau_m) + a_{21}\exp(-\lambda_2\tau_m))/(\lambda_1 - \lambda_2) \quad (1c)$$

$$I_{ct}(\tau_m) = I_{cc}(0)(a_{12}\exp(-\lambda_1\tau_m) + a_{12}\exp(-\lambda_2\tau_m))/(\lambda_1 - \lambda_2) \quad (1d)$$

GraphPad Prism version 4.0 (GraphPad Software Inc., San Diego, CA) was used to simultaneously fit all resolvable peaks within CD147 residues 207–214. Both Ala207 and Gly214 could not be used since their respective *trans* and *cis* resonances exhibited little to no dispersion in the nitrogen dimension.

Recombinant CD147 activity

Recombinant $CD147^{22-205}$ was added to differentiated THP-1 cells at 50, 100, and 200 μg/ml final concentrations for 8 h, and the amount of cytokine released from the cells was measured by sandwich ELISA (ElisaTech, Aurora, CO). THP-1 cells were cultured in RPMI (supplemented with 10% fetal bovine serum) and stored at 37 °C and 5% CO_2 at all times. Differentiation of THP-1 cells was achieved by adding 100 nM phorbol-12-myristate-13-acetate to 1 ml suspended cells in a 24-well cell culture dish at 1 million cells/ml for 24 h, removing undifferentiated cells by aspiration, washing with phosphate-buffered saline, and then replacing the media. The cells were then incubated with CD147, and cytokines secreted into the media were measured by ELISA. ELISAs were performed under the manufacturer's protocol (ElisaTech).

Acknowledgements

This work was funded in part through a National Science Foundation grant to E.E. (grant number MCB-0820567). All NMR experiments collected at 600 and 720 MHz were conducted at the National High Magnetic Field Laboratory supported by cooperative agreement DMR 0654118 between the National Science Foundation and the State of Florida. NMR experiments collected at 900 MHz were conducted at the Rocky Mountain 900 Facility (grant number NIHGM68928). Additionally, a portion of the research was performed using Environmental Molecular Sciences Laboratory, a national scientific user facility sponsored by the Department of Energy's Office of Biological and Environmental Research and located at Pacific Northwest National Laboratory.

Supplementary Data

Supplementary data associated with this article can be found, in the online version, at doi:10.1016/j.jmb.2009.05.080

References

1. Guo, H. M., Majmudar, G., Jensen, T. C., Biswas, C., Toole, B. P. & Gordon, M. K. (1998). Characterization of the gene for human EMMPRIN, a tumor cell surface inducer of matrix metalloproteinases. *Gene*, **220**, 99–108.
2. Schmidt, R., Bültmann, A., Fischel, S., Gillitzer, A., Cullen, P., Walch, A. *et al.* (2008). Extracellular matrix metalloproteinase inducer (CD147) is a novel receptor on platelets, activates platelets, and augments nuclear factor {kappa}B dependent inflammation in monocytes. *Circ. Res.* 107, doi:10.1161/CIRCRESAHA.107.157990.
3. Ruiz, S., Castro-Castro, A. & Bustelo, X. R. (2008). CD147 inhibits the nuclear factor of activated T-cells by impairing vav1 and rac1 downstream signaling. *J. Biol. Chem.* **283**, 5554–5566.
4. Gabison, E. E., Hoang-Xuan, T., Mauviel, A. & Menashi, S. (2005). EMMPRIN/CD147, an MMP modulator in cancer, development and tissue repair. *Biochimie*, **87**, 361–368.
5. Zheng, H. C., Takahashi, H., Murai, Y., Cui, Z. G., Nomoto, K., Miwa, S. *et al.* (2006). Upregulated EMMPRIN/CD147 might contribute to growth and angiogenesis of gastric carcinoma: a good marker for local invasion and prognosis. *Br. J. Cancer*, **95**, 1371–1378.
6. Tang, Y., Nakada, M. T., Kesavan, P., McCabe, F., Millar, H., Rafferty, P. *et al.* (2005). Extracellular matrix metalloproteinase inducer stimulates tumor angiogenesis by elevating vascular endothelial cell growth factor and matrix metal loproteinases. *Cancer Res.* **65**, 3193–3199.
7. Velez, W. & Kyprianou, N. (2007). EMMPRIN is a biomarker of prostate cancer progression in TRAMP mice. *FASEB J.* **21**, A621.
8. Xu, H. Y., Qian, A. R., Shang, P., Xu, J., Kong, L. M., Bian, H. J. & Chen, Z. N. (2007). siRNA targeted against HAb18G/CD147 inhibits MMP-2 secretion, actin and FAK expression in hepatocellular carcinoma cell line via ERK1/2 pathway. *Cancer Lett.* **247**, 336–344.
9. Millimaggi, D., Mari, M., D'Ascenzo, S., Carosa, E., Jannini, E. A., Zucker, S. *et al.* (2007). Tumor vesicle-associated CD147 modulates the angiogenic capability of endothelial cells. *Neoplasia*, **9**, 349–357.
10. Sidhu, S. S., Mengistab, A. T., Tauscher, A. N., LaVail, J. & Basbaum, C. (2004). The microvesicle as a vehicle for EMMPRIN in tumor–stromal interactions. *Oncogene*, **23**, 956–963.
11. Taylor, P. M., Woodfield, R. J., Hodgkin, M. N., Pettitt, T. R., Martin, A., Kerr, D. J. & Wakelam, M. J. O. (2002). Breast cancer cell-derived EMMPRIN stimulates fibroblast MMP2 release through a phospholipase A (2) and 5-lipoxygenase catalyzed pathway. *Oncogene*, **21**, 5765–5772.
12. Zhu, P., Ding, J., Zhou, J., Dong, W. J., Fan, C. M. & Chen, Z. N. (2005). Expression of CD147 on monocytes/macrophages in rheumatoid arthritis: its potential role in monocyte accumulation and matrix metalloproteinase production. *Arthritis Res. Ther.* **7**, R1023–R1033.
13. Zhu, P., Lu, N., Shi, Z. G., Zhou, J., Wu, Z. B., Yang, Y. *et al.* (2006). CD147 overexpression on synoviocytes in rheumatoid arthritis enhances matrix metalloproteinase production and invasiveness of synoviocytes. *Arthritis Res. Ther.* **8**, 1–12.
14. Belton, R. J., Chen, L., Mesquita, F. S. & Nowak, R. A. (2008). Basigin-2 is a cell surface receptor for soluble basigin ligand. *J. Biol. Chem.* **283**, 17805–17814.
15. Yoshida, S., Shibata, M., Yamamoto, S., Hagihara, M., Asai, N., Takahashi, M. *et al.* (2000). Homo-oligomer formation by basigin, an immunoglobulin superfamily member, via its N-terminal immunoglobulin domain. *Eur. J. Biochem.* **267**, 4372–4380.

16. Melchior, A., Denys, A., Deligny, A., Mazurier, J. & Allain, F. (2008). Cyclophilin B induces integrin-mediated cell adhesion by a mechanism involving CD98-dependent activation of protein kinase C-delta and p44/42 mitogen-activated protein kinases. *Exp. Cell Res.* **314**, 616–628.
17. Pakula, R., Melchior, A., Denys, A., Vanpouille, C., Mazurier, J. & Allain, F. (2007). Syndecan-1/CD147 association is essential for cyclophilin B-induced activation of p44/42 mitogen-activated protein kinases and promotion of cell adhesion and chemotaxis. *Glycobiology*, **17**, 492–503.
18. Yurchenko, V., Constant, S. & Bukrinsky, M. (2006). Dealing with the family: CD147 interactions with cyclophilins. *Immunology*, **117**, 301–309.
19. Andreotti, A. H. (2003). Native state proline isomerization: an intrinsic molecular switch. *Biochemistry*, **42**, 9515–9524.
20. Yao, Q. Z., Li, M., Yang, H., Chai, H., Fisher, W. & Chen, C. Y. (2005). Roles of cyclophilins in cancers and other organ systems. *World J. Surg.* **29**, 276–280.
21. Pap, T. (2005). Cyclophilins in rheumatoid arthritis—stepping into an undiscovered country? *Clin. Immunol.* **116**, 199–201.
22. Billich, A., Winkler, G., Aschauer, H., Rot, A. & Peichl, P. (1997). Presence of cyclophilin A in synovial fluids of patients with rheumatoid arthritis. *J. Exp. Med.* **185**, 975–980.
23. Yurchenko, V., O'Connor, M., Dai, W. W., Guo, H. M., Toole, B., Sherry, B. & Bukrinsky, M. (2001). CD147 is a signaling receptor for cyclophilin B. *Biochem. Biophys. Res. Commun.* **288**, 786–788.
24. Yurchenko, V., Zybarth, G., O'Connor, M., Dai, W. W., Franchin, G., Hao, T. *et al.* (2002). Active site residues of cyclophilin A are crucial for its signaling activity via CD147. *J. Biol. Chem.* **277**, 22959–22965.
25. Jin, Z. G., Lungu, A. O., Xie, L., Wang, M., Wong, C. & Berk, B. C. (2004). Cyclophilin A is a proinflammatory cytokine that activates endothelial cells. *Arterioscler. Thromb. Vasc. Biol.* **24**, 1186–1191.
26. Arora, K., Gwinn, W. M., Bower, M. A., Watson, A., Okwumabua, I., MacDonald, H. R. *et al.* (2005). Extracellular cyclophilins contribute to the regulation of inflammatory responses. *J. Immunol.* **175**, 517–522.
27. Gwinn, W. M., Damsker, J. M., Falahati, R., Okwumabua, I., Kelly-Welch, A., Keegan, A. D. *et al.* (2006). Novel approach to inhibit asthma-mediated lung inflammation using anti-CD147 intervention. *J. Immunol.* **177**, 4870–4879.
28. Damsker, J. M., Okwumabua, I., Bukrinsky, M. I. & Constant, S. L. (2006). Contribution of cyclophilin–CD147 interactions in rheumatoid arthritis. *J. Immunol.* **176**, S47.
29. Bose, S., Mathur, M., Bates, P., Joshi, N. & Banerjee, A. K. (2003). Requirement for cyclophilin A for the replication of vesicular stomatitis virus New Jersey serotype. *J. Gen. Virol.* **84**, 1687–1699.
30. Castro, A. P. V., Carvalho, T. M. U., Moussatche, N. & Damaso, C. R. A. (2003). Redistribution of cyclophilin A to viral factories during vaccinia virus infection and its incorporation into mature particles. *J. Virol.* **77**, 9052–9068.
31. Sorin, M. & Kalpana, G. V. (2006). Dynamics of virus–host interplay in HIV-1 replication. *Curr. HIV Res.* **4**, 117–130.
32. Chen, Z. N., Mi, L., Xu, J., Yu, J. Y., Wang, X. H., Jiang, J. L. *et al.* (2005). Function of HAb18G/CD147 in invasion of host cells by severe acute respiratory syndrome coronavirus. *J. Infect. Dis.* **191**, 755–760.
33. Pushkarsky, T., Zybarth, G., Dubrovsky, L., Yurchenko, V., Tang, H., Guo, H. M. *et al.* (2001). CD147 facilitates HIV-1 infection by interacting with virus-associated cyclophilin A. *Proc. Natl Acad. Sci. USA*, **98**, 6360–6365.
34. Yu, X. L., Hu, T., Du, J. M., Ding, J. P., Yang, X. M., Zhang, J. *et al.* (2008). Crystal structure of HAb18g/CD147—implications for immunoglobulin superfamily homophilic adhesion. *J. Biol. Chem.* **283**, 18056–18065.
35. Yang, H., Chen, J., Yang, J., Qiao, S., Zhao, S. & Yu, L. (2007). Cyclophilin A is upregulated in small cell lung cancer and activates ERK1/2 signal. *Biochem. Biophys. Res. Commun.* **361**, 763–767.
36. Bosco, D. A., Eisenmesser, E. Z., Pochapsky, S., Sundquist, W. I. & Kern, D. (2002). Catalysis of *cis/trans* isomerization in native HIV-1 capsid by human cyclophilin A. *Proc. Natl Acad. Sci. USA*, **99**, 5247–5252.
37. Campos-Olivas, R. & Summers, M. F. (1999). Backbone dynamics of the N-terminal domain of the HIV-1 capsid protein and comparison with the G94D mutant conferring cyclosporin resistance/dependence. *Biochemistry*, **38**, 10262–10271.
38. Sun, J. X. & Hemler, M. E. (2001). Regulation of MMP-1 and MMP-2 production through CD147/extracellular matrix metalloproteinase inducer interactions. *Cancer Res.* **61**, 2276–2281.
39. Jia, L., Wang, H. J., Zhou, H. M., Cao, J., Hu, Y. C. & Zhang, J. N. (2006). Caveolin-1 up-regulates CD 147 glycosylation and the invasive capability of murine hepatocarcinoma cell lines. *Int. J. Biochem. Cell Biol.* **38**, 1584–1593.
40. Jia, L., Zhou, H. M., Wang, S. J., Cao, J., Wei, W. & Zhang, J. N. (2006). Deglycosylation of CD147 down-regulates matrix metalloproteinase-11 expression and the adhesive capability of murine hepatocarcinoma cell HcaF in vitro. *IUBMB Life*, **58**, 209–216.
41. Markovic, I., Stantchev, T. S., Fields, K. H., Tiffany, L. J., Tomic, M., Weiss, C. D. *et al.* (2004). Thiol/disulfide exchange is a prerequisite for CXCR4-tropic HIV-1 envelope-mediated T-cell fusion during viral entry. *Blood*, **103**, 1586–1594.
42. Iacono, K. T., Brown, A. L., Greene, M. I. & Saouaf, S. J. (2007). CD147 immunoglobulin superfamily receptor function and role in pathology. *Exp. Mol. Pathol.* **83**, 283–295.
43. Cornilescu, G., Delaglio, F. & Bax, A. (1999). Protein backbone angle restraints from searching a database for chemical shift and sequence homology. *J. Biomol. NMR*, **13**, 289–302.
44. Larsson, G., Martinez, G., Schleucher, J. & Wijmenga, S. S. (2003). Detection of nano-second internal motion and determination of the overall tumbling times independent of the time scale of internal motion in proteins from NMR relaxation data. *J. Biomol. NMR*, **27**, 291–312.
45. Cole, R. & Loria, J. P. (2003). FAST-Modelfree: a program for rapid automated analysis of solution NMR spin-relaxation data. *J. Biomol. NMR*, **26**, 203–213.
46. Yurchenko, V., Pushkarsky, T., Li, J. H., Dai, W. W., Sherry, B. & Bukrinsky, M. (2005). Regulation of CD147 cell surface expression—involvement of the proline residue in the CD147 transmembrane domain. *J. Biol. Chem.* **280**, 17013–17019.
47. Hanoulle, X., Melchior, A., Sibille, N., Parent, B., Denys, A., Wieruszeski, J. M. *et al.* (2007). Structural and functional characterization of the interaction between cyclophilin B and a heparin-derived oligosaccharide. *J. Biol. Chem.* **282**, 34148–34158.

48. Ottiger, M., Zerbe, O., Guntert, P. & Wuthrich, K. (1997). The NMR solution conformation of unligated human cyclophilin A. *J. Mol. Biol.* **272**, 64–81.
49. Eisenmesser, E. Z., Bosco, D. A., Akke, M. & Kern, D. (2002). Enzyme dynamics during catalysis. *Science*, **295**, 1520–1523.
50. Piotukh, K., Gu, W., Kofler, M., Labudde, D., Helms, V. & Freund, C. (2005). Cyclophilin a binds to linear peptide motifs containing a consensus that is present in many human proteins. *J. Biol. Chem.* **280**, 23668–23674.
51. Brazin, K. N., Mallis, R. J., Fulton, D. B. & Andreotti, A. H. (2002). Regulation of the tyrosine kinase Itk by the peptidyl–prolyl isomerase cyclophilin A. *Proc. Natl Acad. Sci. USA*, **99**, 1899–1904.
52. Grathwohl, C. & Wuthrich, K. (1981). NMR studies of the rates of proline *cis–trans* isomerization in oligopeptides. *Biopolymers*, **20**, 2623–2633.
53. Liu, J., Chen, C. M. & Walsh, C. T. (1991). Human and *Escherichia coli* cyclophilins—sensitivity to inhibition by the immunosuppressant cyclosporin A correlates with a specific tryptophan residue. *Biochemistry*, **30**, 2306–2310.
54. Hanna, S. M., Kirk, P., Holt, O. J., Puklavec, M. J., Brown, M. H. & Barclay, A. N. (2003). A novel form of the membrane protein CD147 that contains an extra Ig-like domain and interacts homophilically. *BMC Biochem.* **4**, 17.
55. Kern, D., Kern, G., Scherer, G., Fischer, G. & Drakenberg, T. (1995). Kinetic analysis of cyclophilin-catalyzed prolyl *cis/trans* isomerization by dynamic NMR spectroscopy. *Biochemistry*, **34**, 13594–13602.
56. Yap, A. S., Crampton, M. S. & Hardin, J. (2007). Making and breaking contacts: the cellular biology of cadherin regulation. *Curr. Opin. Cell Biol.* **19**, 508–514.
57. Guerrini, M., Hricovini, M. & Torri, G. (2007). Interaction of heparins with fibroblast growth factors: conformational aspects. *Curr. Pharm. Des.* **13**, 2045–2056.
58. Wilson, M. C., Meredith, D., Fox, J. E. M., Manoharan, C., Davies, A. J. & Halestrap, A. P. (2005). Basigin (CD147) is the target for organomercurial inhibition of monocarboxylate transporter isoforms 1 and 4—the ancillary protein for the insensitive MCT2 is embigin (gp70). *J. Biol. Chem.* **280**, 27213–27221.
59. Barclay, A. N. & Brown, M. H. (2006). The SIRP family of receptors and immune regulation. *Nat. Rev. Immunol.* **6**, 457–464.
60. Lands, W. E. M. (1998). A review of alcohol clearance in humans. *Alcohol*, **15**, 147–160.
61. Ke, H., Mayrose, D. & Cao, W. (1993). Crystal structure of cyclophilin A complexed with substrate Ala-Pro suggests a solvent-assisted mechanism of *cis–trans* isomerization. *Proc. Natl Acad. Sci. USA*, **90**, 3324–3328.
62. Zhao, Y. & Ke, H. (1996). Crystal structure implies that cyclophilin predominantly catalyzes the *trans* to *cis* isomerization. *Biochemistry*, **35**, 7356–7361.
63. Eisenmesser, E. Z., Millet, O., Labeikovsky, W., Korzhnev, D. M., Wolf-Watz, M., Bosco, D. A. *et al.* (2005). Intrinsic dynamics of an enzyme underlies catalysis. *Nature*, **438**, 117–121.
64. Pushkarsky, T., Yurchenko, V., Laborico, A. & Bukrinsky, M. (2007). CD147 stimulates HIV-1 infection in a signal-independent fashion. *Biochem. Biophys. Res. Commun.* **363**, 495–499.
65. Delaglio, F., Grzesiek, S., Vuister, G. W., Zhu, G., Pfeifer, J. & Bax, A. (1995). NMRPipe—a multidimensional spectral processing system based on UNIX pipes. *J. Biomol. NMR*, **6**, 277–293.
66. Vranken, W. F., Boucher, W., Stevens, T. J., Fogh, R. H., Pajon, A., Llinas, P. *et al.* (2005). The CCPN data model for NMR spectroscopy: development of a software pipeline. *Proteins: Struct., Funct., Bioinform.* **59**, 687–696.
67. Sattler, M., Schleucher, J. & Griesinger, C. (1999). Heteronuclear multidimensional NMR experiments for the structure determination of proteins in solution employing pulsed field gradients. *Prog. Nucl. Magn. Reson. Spectrosc.* **34**, 93–158.
68. d'Auvergne, E. J. & Gooley, P. R. (2008). Optimisation of NMR dynamic models. I. Minimisation algorithms and their performance within the model-free and Brownian rotational diffusion spaces. *J. Biomol. NMR*, **40**, 107–119.
69. Farrow, N. A., Zhang, O. W., Formankay, J. D. & Kay, L. E. (1994). A heteronuclear correlation experiment for simultaneous determination of N-15 longitudinal decay and chemical-exchange rates of systems in slow equilibrium. *J. Biomol. NMR*, **4**, 727–734.
70. Farrow, N. A., Zhang, O. W., Formankay, J. D. & Kay, L. E. (1995). Comparison of the backbone dynamics of a folded and an unfolded Sh3 domain existing in equilibrium in aqueous buffer. *Biochemistry*, **34**, 868–878.
71. Sarkar, P., Reichman, C., Saleh, T., Birge, R. B. & Kalodimos, C. G. (2007). Proline *cis–trans* isomerization controls autoinhibition of a signaling protein. *Mol. Cell*, **25**, 413–426.